Above-water measurements of reflectance and chlorophyll-a algorithms in the Gulf of Lions, NW Mediterranean Sea

S. Ouillon, Anne Petrenko

Above-water measurements of reflectance and chlorophyll-a algorithms in the Gulf of Lions, NW Mediterranean Sea

Sylvain Ouillon

Institut de Recherche pour le Développement, UR 103
BP A5, 98848 Nouméa cedex, New Caledonia
ouillon@noumea.ird.nc

Anne A. Petrenko

Laboratoire d'Océanographie et de Biogéochimie, CNRS,
Centre d'Océanologie de Marseille, Luminy, 13288 Marseille cedex 09, France
anne.petrenko@com.univ-mrs.fr

Abstract: Above-water reflectance and surface chlorophyll *a* concentrations (Chl a) were measured in the Gulf of Lions, northwestern Mediterranean Sea in 2000 and 2001 in order to test Chl a inversion algorithms. Surface waters were separated in Case 2 waters in the Rhône River plume and proximal Region of Freshwater Influence (ROFI) stations, and Case 1 waters at all the other stations. Case 2 waters were characterized by R443/R555 < R443/R510 < R490/R555 < R490/R510 < 1. In the first part, we compared the concurrent reflectance measurements made with a scanning polarization radiometer (SIMBAD) and a hyperspectral Ocean Optics radiometer. The comparison of the remote-sensing reflectance (Rrs) values at SIMBAD wavelengths shows excellent agreement for Rrs values higher than 0.01 sr^{-1}. Between the two instruments, reflectance ratios, commonly used in Chl a algorithms, show differences smaller than 2% in the Case 2 waters, and smaller than 20% in the Case 1 waters. In the second part, concurrent measurements of Chl a and of hyperspectral reflectance from 6 cruises were used to analyze the statistical performance of global (OC2, OC4) and regional regression algorithms using mainly SeaWiFS bands. The algorithms were tested first over the entire domain, then separately over the Case 1 and Case 2 waters. Chl a algorithms using band ratios such as the one presented in Bricaud et al. (2002) are suitable for the Case 1 waters. However, taking into account the large dispersion of Chl a for very close reflectance ratios in the Case 2 waters, single band ratios are not suitable for deriving Chl a. The use of a 4-wavelength parameter such as X_c, defined by Tassan (1994), leads to better results in the plume and proximal Rhône ROFI.

OCIS codes: (010.4450) Ocean optics; (280.0280) Remote Sensing

References and links

1. J.A. Yoder, C.R. McClain, G.C. Feldman, and W. Esaias, "Annual cycles of phytoplankton chlorophyll concentrations in the global ocean: a satellite view," Glob. Biogeoch. Cycles **7**, 181-193 (1993).
2. W.W. Gregg, and M.E. Conkright, "Global seasonal climatologies of ocean chlorophyll: blending in situ and satellite data for the CZCS era," J. Geoph. Res. **106**, 2499-2515 (2001).
3. A. Bricaud, E. Bosc, and D. Antoine, "Algal biomass and sea surface temperature in the Mediterranean Basin, Intercomparison of data from various sensors, and implications for primary production estimates," Remote Sens. Env. **81**, 163-178 (2002).
4. W.W. Gregg, M.E. Conkright, P. Ginoux, J.E. O'Reilly, and N.W. Casey, "Ocean primary production and

#6654 - $15.00 US Received 23 February 2005; revised 13 March 2005; accepted 21 March 2005

climate: Global decadal changes," Geoph. Res. Let. **30**, 1809 (2003)
5. C.D. Mobley, "Estimation of the remote-sensing reflectance from above-surface measurements," Appl. Opt. **38**, 7442–7455 (1999).
6. S.B. Hooker, and S. Maritorena, "An evaluation of oceanographic radiometers and deployment methodologies," J. Atm. Ocean. Techn. **17**, 811-830 (2000).
7. G.S. Fargion, and J.L. Mueller (Eds.), *Ocean Optics for satellite ocean color sensor validation, rev. 2* (NASA, Greenbelt, 2000).
8. J.L. Mueller, C. Davis, R. Arnone, R. Frouin, K. Carder, Z.P. Lee, R.G. Steward, S. Hooker, C.D. Mobley, and S. McLean, "Above-water radiance and remote sensing reflectance measurement and analysis protocols," in *Ocean Optics for satellite ocean color sensor validation, rev. 2,* G.S. Fargion and J.L. Mueller, eds. (NASA, Greenbelt, MD, 2000), pp 98-107.
9. M. Kishino, T. Ishimaru, K. Furuya, T. Oishi, and K. Kawasaki, "In-water algorithms for DEOS/OCTS," J. Ocean. **54**, 383-399 (1998).
10. J.E. O'Reilly, S. Maritorena, G.G. Mitchell, D.A. Siegel, K.L. Carder, S.A. Garver, M. Kahru, andC. McClain,. "Ocean color algorithms for SeaWiFS," J. Geoph. Res. **103**, 24937-24953 (1998).
11. J.E. O'Reilly, S. Maritorena, D.A. Siegel, M. O'Brien, D. Toole, B.G. Mitchell, M. Kahru, F.P. Chavez, P. Strutton, G.F. Cota, S.B. Hooker, C. McClain, K.L. Carder, F. Müeller-Karger, L. Harding, A. Magnuson, D. Phinney, G.F. Moore, J. Aiken, K.R. Arrigo, R. Letelier, and M. Culver, "Ocean color chlorophyll a algorithms for SeaWiFS, OC2, and OC4: Version 4," in *SeaWiFS Postlaunch Technical Report Series, Vol. 11: Seawifs Postlaunch Calibration and Validation Analyses Part 3,* S.B. Hooker and E.R. Firestone, eds. (NASA, Greenbelt, MD, 2000), pp. 9-23.
12. M. Kahru, and B.G. Mitchell, "Empirical chlorophyll algorithm and preliminary SeaWiFS validation for the California Current," Int. J. Remote Sens. **20**, 3423-3429 (1999).
13. E.J. D'Sa, J.B. Zaitzeff, and R.G. Steward, "Monitoring water quality in Florida Bay with remotely sensed salinity and in situ bio-optical observations," Int. J. Remote Sens. **21**, 811-816 (2000).
14. A. Gitelson, A. Karnieli, N. Goldman, Y.Z. Yacobi, and M. Mayo, "Chlorophyll estimation in the southeastern Mediterranean using CZCS images: adaptation of an algorithm and its validation," J. Mar. Syst. **9**, 283-290 (1996).
15. F. D'Ortenzio, S. Marullo, M. Ragni, M. Ribera d'Alcalà, and R. Santoleri, "Validation of empirical SeaWiFS algorithms for chlorophyll-a retrieval in the Mediterranean Sea, A case study for oligotrophic seas," Remote Sens. Env. **82**, 79-94 (2002).
16. A. Morel, and J.M. André, "Pigment distribution and primary production in the western Mediterranean as derived and modelled from coastal zone color scanner observations," J. Geoph. Res. **96**, 12685-12698 (1991).
17. D. Antoine, A. Morel, and J.M. André, "Algal pigment distribution and primary production in the Eastern Mediterranean as derived from coastal zone color scanner observations," J. Geoph. Res. **100**, 16193-16209 (1995).
18. H. Claustre, A. Morel, S.B. Hooker, M. Babin, D. Antoine, K. Oubelkheir, A. Bricaud, K. Leblanc, B. Quéguiner, and S. Maritorena, "Is desert dust making oligotrophic waters greener?," Geoph. Res. Let. **29**, 107 (2002).
19. S. Tassan, "Local algorithms using SeaWiFS data for the retrieval of phytoplankton, pigments, suspended sediment, and yellow substance in coastal waters," Appl. Opt. **33**, 2369-2378 (1994).
20. A. Morel, A. Bricaud, J.M. André, and J. Pelaez-Hudlet, "Spatial-temporal evolution of the Rhône river plume as seen by CZCS imagery: Consequences upon primary productions in the Gulf of Lions," in *EROS 2000*, J.M. Martin and H. Barth, eds. (Europ. Comm., Brussels, 1990), pp 45-62.
21. J.H. Simpson, "Physical processes in the ROFI regime," J. Mar. Syst. **12**, 3-15 (1997).
22. G. Jacques, H.J. Minas, M. Minas, and P. Nival, "Influence des conditions hivernales sur les productions phyto et zooplanctoniques en Méditerranée nord-occidentale, II. Biomasse et production planctonique," Mar. Biol. **23**, 251-265 (1973).
23. J.P. Béthoux, and B. Gentili, "The Mediterranean Sea, coastal and deep-sea signatures of climatic and environmental changes," J. Mar. Syst. **7**, 383-394 (1996).
24. A. Monaco, X. Durrieu de Madron, O. Radakovitch, S. Heussner, and J. Carbonne, "Origin and variability of downward biogeochemical fluxes on the Rhone continental margin (NW Mediterranean)," Deep-Sea Res. I **46**, 1483-1511 (1999).
25. C. Millot, "The Gulf of Lion's hydrodynamics," Cont. Shelf Res. **10**, 885-894 (1990).
26. A.A. Petrenko, "Variability of circulation features in the Gulf of Lion NW Mediterranean Sea. Importance of inertial currents," Ocean. Acta **26**, 323-338 (2003).
27. J.M. Beckers, P. Brasseur, and J.C.J. Nihoul, "Circulation of the western Mediterranean: from global to regional scales," Deep-Sea Res. II **44**, 531-549 (1997).
28. C. Millot, "Review paper: Circulation in the Western Mediterranean Sea," J. Mar. Syst. **20**, 423-442 (1999).
29. D. Lefèvre, H.J. Minas, M. Minas, C. Robinson, P.J. le B. Williams, and E.M.S. Woodward, "Review of gross community production, primary production, net community production and dark community respiration in the Gulf of Lions," Deep-Sea Res. II **44**, 801-832 (1997).
30. J.E. Salisbury, J.W. Campbell, L.D. Meeker, and C. Vörösmarty, "Ocean color and river data reveal fluvial influence in coastal waters," EOS Transactions **82**, 221 (2001).
31. P. Treguer, and P. Le Corre, *Manuel d'analyse des sels nutritifs dans l'eau de mer (utilisation de l'Auto-Analyseur II Technicon)* (Université de Bretagne Occidentale, Brest, France, 1975).

#6654 - $15.00 US Received 23 February 2005; revised 13 March 2005; accepted 21 March 2005

32. N.A. Welschmeyer, "Fluorimetric analysis of chlorophyll a in the presence of chlorophyll b and pheopigments," Limnol. Ocean. **39**, 1985-1992 (1994).
33. A. Herbland, A. Le Bouteiller, and P. Raimbault, "Size structure of phytoplankton biomass in the equatorial Atlantic Ocean," Deep Sea Res. A **32**, 819-836 (1985).
34. M.A. Lodhi, and D.C. Rundquist, "A spectral analysis of bottom-induced variation in the colour of Sand Hills lakes, Nebraska, USA," Int. J. Remote Sens. **22**, 1665-1682 (2001).
35. F. Lahet, S. Ouillon, and P. Forget, "Colour classification of coastal waters of Ebro river plume from spectral reflectances," Int. J. Remote Sens. **22**, 1639-1664 (2001).
36. E. Hochberg, M.J. Atkinson, and S. Andréfouët, "Spectral reflectance of coral-reef bottom types worldwide and implications for coral reef remote sensing," Remote Sens. Env. **85**, 159-173 (2003).
37. E.M. Louchard, R.P. Reid, C.F. Stephens, C. Davis, R. Leathers, and T. Downes, "Optical remote sensing of benthic habitats and bathymetry in coastal environments at Lee Stocking Island, Bahamas: A comparative spectral classification approach," Limnol. Ocean. **48**, 511-521 (2003).
38. G. Dall'Olmo, A.A. Gitelson, and D.C. Rundquist, "Towards a unified approach for remote estimation of chlorophyll-a in both terrestrial vegetation and turbid productive waters," Geoph. Res. Let. **30**, 1938 (2003).
39. K. Masuda, and T. Takashima, "The effect of solar zenith angle and surface wind speed on water surface reflectivity," Remote Sens. Env. **57**, 58-62 (1996).
40. B. Fougnie, R. Frouin, P. Lecomte, and P.-Y. Deschamps, "Reduction of skylight reflection effects in the above-water measurements of marine diffuse reflectances," Appl. Opt. **38**, 3844-3856 (1999).
41. P. Forget, and S. Ouillon, "Surface suspended matter off the Rhône river mouth from visible satellite imagery," Ocean. Acta **21**, 739-749 (1998).
42. J.M. Froidefond, L. Gardel, D. Guiral, M. Parra, and J.F. Ternon, "Spectral remote sensing reflectances of coastal waters in French Guiana under the Amazon influence," Remote Sens. Env. **80**, 225-232 (2002).
43. D.A. Toole, D.A. Siegel, D.W. Menzies, M.J. Neumann, and R.C. Smith, "Remote-sensing reflectance determinations in the coastal ocean environment: impact of instrumental characteristics and environmental variability," Appl. Opt. **39**, 456-469 (2000).
44. M. Darecki, and D. Stramski, "An evaluation of MODIS and SeaWiFS bio-optical algorithms in the Baltic Sea," Rem. Sens. Env. **89**, 326-350 (2004).
45. A. Cunningham, P. Wood, and K. Jones, "Reflectance properties of hydrographically and optically stratified fjords (Scottish sea lochs) during the Spring diatom bloom," Int. J. Remote Sens. **22**, 2885-2897 (2001).
46. J.J. Naudin, G. Cauwet, C. Fajon, L. Oriol, S. Terzic, J.L. Devenon, and P. Broche, "Effect of mixing on microbial communities in the Rhone River plume," J. Mar. Syst. **28**, 203-227 (2001).
47. K.L. Carder, R.G. Steward, G.R. Harvey, and P.B. Ortner, "Marine humic and fulvic acids: their effects on remote sensing of ocean chlorophyll," Limnol. Ocean. **34**, 68-81 (1989).
48. D.G. Bowers, G.E.L. Harker, and B. Stephan, "Absorption spectra of inorganic particles in the Irish Sea and their relevance to remote sensing of chlorophyll," Int. J. Remote Sens. **17**, 2449-2460 (1996).
49. F. Lahet, S. Ouillon, and P. Forget, "A three component model of ocean colour and its application in the Ebro River mouth area," Remote Sens. Envir. **72**, 181-190 (2000).
50. Y.H. Ahn, J.E. Moon, and S. Gallegos, "Development of suspended particulate matter algorithms for ocean color remote sensing," Kor. J. Remote Sens. **17**, 285-295 (2001).
51. S. Ouillon, P. Douillet, and S. Andréfouët, "Coupling satellite data with in situ measurements and numerical modeling to study fine suspended sediment transport: a study for the lagoon of New Caledonia," Coral Reefs **23**, 109-122 (2004).
52. N. Hoepffner, and S. Sathyendranath, "Bio-optical characteristics of coastal waters: Absorption spectra of phytoplankton and pigment distribution in the western North Atlantic," Limnol. Ocean. **37**, 1660-1679 (1992).
53. C.D. Mobley, and D. Stramski, "Effects of microbial particles on oceanic optics: Methodology for radiative transfer modeling and example simulations," Limnol. Ocean. **42**, 550-560 (1997).
54. D. Stramski, and C.D. Mobley, "Effects of microbial particles on oceanic optics: A database of single-particle optical properties," Limnol. Ocean. **42**, 538-549 (1997).
55. J.T.O. Kirk, *Light and photosynthesis in aquatic ecosystems* (Cambridge Univ. Press, 1994).
56. V.F. Banzon, R.H. Evans, S. Marullo, R. Santoleri, and F. D'Ortenzio, "SeaWiFS observations of the southern Adriatic sea bloom (1998-2000): the role of atmospherically-forced deep convection, " presented at the Seventh International Conference on Remote Sensing for Marine and Coastal Environments, Miami, Florida, 20-22 May 2002.
57. F. Lahet, P. Forget, and S. Ouillon, "Application of a colour classification method to quantify the constituents of coastal waters from *in situ* reflectances sampled at satellite sensor wavebands," Int. J. Remote Sens. **22**, 909-914 (2001).

1. Introduction

The quantification of spatial and temporal variability of phytoplankton biomass has improved dramatically since the early ocean color satellite images. The study of the influence of climate changes and anthropogenic inputs on algal biomass and primary production has also radically changed with satellite datasets. Data provided by the Coastal Zone Color Scanner (CZCS)

#6654 - $15.00 US Received 23 February 2005; revised 13 March 2005; accepted 21 March 2005

sensor from 1978 to 1986, among others, have been used to study the seasonal variations in algal biomass (e.g., Ref. [1-2]). With the availability of recent multispectral sensors, such as the Sea-viewing Wide Field-of-view Sensor (SeaWiFS), the Ocean Color and Temperature Scanner (OCTS), it is now possible to estimate their inter-annual variability (e.g., Ref. [3-4]). Nonetheless, the study of coastal areas requires not only a high spectral resolution, but also a spatial resolution higher than the one the above sensors can provide. The Medium Resolution Imaging Spectrometer (MERIS) and the Moderate Resolution Imaging Spectroradiometer (MODIS) sensors should be particularly well adapted to coastal studies.

Along with these new satellite sensors and the increasing number of field calibration multispectral or hyperspectral radiometers, *in situ* ocean measurement techniques and algorithms are continuously being developed, compared and improved (e.g., Ref. [5-6]). Efforts to obtain standard measurement protocols have been made in order to improve measurement consistency and allow inter-comparisons [7]. Concerning the above-water reflectance measurements, Mueller et al. [8] recommended protocols adapted to the different radiometer types. In parallel with instrumental and methodological improvements, general chlorophyll *a* inversion algorithms have been developed from large field and satellite datasets [9-11]. For example, the field dataset used to establish the SeaWiFS inversion algorithms is based on 2804 measurements from a great variety of bio-optical zones [11]. Nonetheless, various authors have stressed the necessity for establishing local inversion algorithms, specific to areas with non standard optical properties, such as the California Current [12], the Gulf of Mexico [13] or the Mediterranean Sea [14-15].

The Mediterranean Sea is a typical example where general inversion algorithms need further work. Remote sensing has been used to analyze the phytoplankton biomass and the primary production within the entire Mediterranean Sea or within parts of it since the 1980's using CZCS data ([16] in the Western Mediterranean Basin; [17] in the Eastern Mediterranean Basin). In the Mediterranean Sea, the general inversion algorithms need to be improved at chlorophyll *a* concentrations (hereafter noted "Chl a") below 0.2 $mg.m^{-3}$ [3; 14] and in Case 2 waters. This was partially explained [3; 18], and specific inversion algorithms were adapted locally or regionally: Tassan [19] used data gathered in the Gulf of Naples, Italy; Antoine et al. [17] focused on the Eastern Mediterranean Basin; Gitelson et al. [14] used data collected along a transect from Gaza to the open sea; D'Ortenzio et al. [15] considered data from Case 1 waters in the Sicily Channel, in the Ionian Sea and in the northwestern Mediterranean; Bricaud et al. [3] studied the entire Mediterranean Sea divided into 13 regions.

The goal of the present study is to test the need for specific local algorithms in a coastal area of the Mediterranean Sea. We focus on one of the 3 most productive regions from the 13 defined by Bricaud et al. [3]: the Gulf of Lions, in the northwestern Mediterranean Sea. The Gulf of Lions receives fresh and nutrient-rich waters from the Rhône River and is a very productive region during blooms [20]. This article starts with the descriptions of: the site (Section 2.1), the oceanographic cruises (Section 2.2), the radiometers used for the above-water measurements and the protocols used to derive reflectance values (Section 2.3). Section 3 describes the location and type of waters encountered during the study. Measurements with two different radiometers are compared in Section 4. Then regional and local Chl a algorithms are tested and new ones proposed (Section 5). This is followed with discussion and conclusions (Section 6). By restricting our optical measurements to above-water reflectance values, we were able to cover a large area nearly synoptically. This strategy is particularly well adapted to rapidly changing environments such as river mouths and plume areas. Our study site includes the Rhône River plume. One of the main results of this study shows that different algorithms need to be used for the proximal zone and the distal zone of the Region of Freshwater Influence ('ROFI' as introduced by Simpson [21]).

2. Study area, material, and methods

2.1. Study area

The Mediterranean Sea is a microtidal and oligotrophic semi-enclosed sea. Mediterranean

#6654 - $15.00 US Received 23 February 2005; revised 13 March 2005; accepted 21 March 2005

waters receive significant land-derived inputs of natural and anthropogenic constituents and show strong seasonal variations in some areas (e.g., Ref. [22-23]). The Gulf of Lions (Fig. 1; see also location in [3], Fig. 1, and bathymetry in [24], Fig. 1) is a complex hydrological area located in the northwest of the western Mediterranean Sea. It receives freshwater from the Rhône River, surface North Atlantic water from the Northern Current [25-26] and is subject to intense vertical mixing. Circulation in the Western Mediterranean Sea was described in Beckers et al. [27] and in Millot [28]. Millot [25] showed the hydrodynamic features specific to the Gulf of Lions. Lefevre et al. [29] showed the existence of 4 hydrological provinces in the Gulf of Lions: (i) the Gulf of Marseilles, a coastal oligotrophic system, (ii) the Rhône River plume, containing high levels of nutrients, (iii) the highly productive area located west of the plume, and (iv) the southern area including the oligotrophic Northern Current, a frontal zone of high primary production and a divergence area. As shown by Lefevre et al. [29], the fertility of each of these water bodies is different, and hydrology is the major component determining the biological populations. The Gulf of Lions exhibits a strong seasonal variability. In winter, the lack of water column stratification and the strong variability of currents favor vertical exchanges, and hence nutrient availability [24]. Phytoplankton biomass production is also strongly stimulated by riverine nutrient inputs. Seasonal variability in fluvial inputs generates variability in phytoplankton biomass, with a time lag of several days to weeks [30].

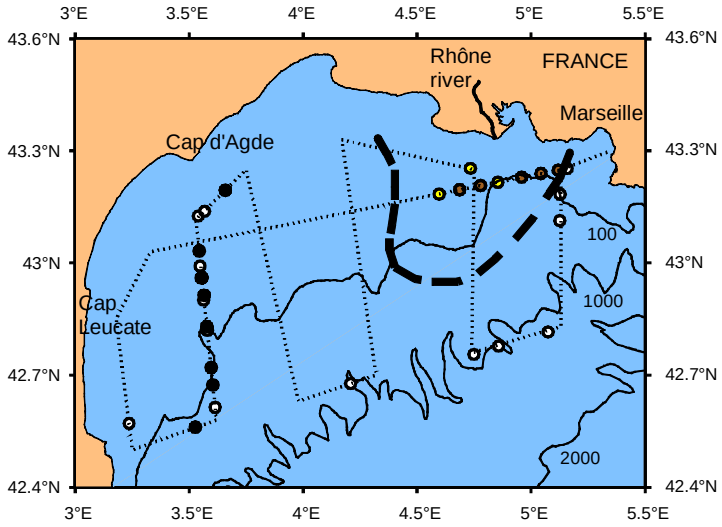

Fig. 1. Map of the Gulf of Lions with isobaths at 100, 1000, and 2000 m. The dotted line indicates the SARHYGOL trajectory. The optical stations are indicated by circles, with black or brown circles when both Ocean Optics and Simbad measurements were collected. Brown and yellow circles correspond to Case 2 waters. The dashed line indicates the approximate boundary between the proximal zone and the distal zone of the Rhône ROFI.

2.2. Field campaigns and in situ Chl a data

A series of seasonal short cruises (SARHYGOL, French acronym for "Regular and Automatic Survey of Hydrodynamics in the Gulf of Lions") were initiated in 2000 to survey hydrodynamics and water quality across the Gulf of Lions, as part of the French scientific programmes '*Programme National Environnement Cotier*' (PNEC, *Chantier Golfe du Lion*) and '*Programme ATmosphere Ocean à Moyenne échelle*' (PATOM). Continuous measurements were performed during each cruise: horizontal currents were measured using a hull-mounted ADCP (Acoustic Doppler Current Profiler), and surface temperature, salinity and fluorescence were recorded using a Seabird thermosalinograph and a Turner fluorometer linked to a pumping system. Every half hour, surface water samples were collected to

#6654 - $15.00 US Received 23 February 2005; revised 13 March 2005; accepted 21 March 2005

determine nutrient concentrations [31], and the *in vitro* Chl a was determined using a fluorometric method [32] after a methanol extraction [33]. In order to get a near synchronous view of the circulation, the entire gulf was covered in ~ 48 hours (Fig. 1) and, for current data quality, the 25-m long RV Téthys II cruised at a constant speed not exceeding 8 knots. With these constraints, it was not possible to stop the vessel and thus to perform underwater optical measurements. So, in order to calibrate satellite images over the Gulf of Lions, the data set was completed with above-water optical measurements.

2.3. Optical measurements

Two different kinds of above-water measurements of reflectance were collected and compared: hyperspectral measurements using an Ocean Optics SD1000 radiometer, and multispectral measurements using the SIMBAD radiometer, an instrument that includes a polarizer.

The Ocean Optics SD1000 or SD2000 UV-VIS spectrometer has been used by several authors on Case 2 waters or over sea bottom (e.g. Ref. [34-38]). Our SD1000 equipment (field of view = 22°) has 1024 channels ranging from 410 to 900 nm. A 25-m long optic fiber makes it possible to measure directly or indirectly solar downwelling irradiance E_d, upwelling radiance L_u and sky radiance L_{sky}. Mobley's protocol [5] was used: measurements were performed with a nadir angle of 40° and an azimuth viewing direction of 135° (with an accuracy of ± 5°), so as to minimize the reflection at the sea surface. This protocol agrees with the recommendations of Mueller et al. [8]. Downwelling irradiance E_d was calculated from the downwelling radiance measured on a white plate made of Spectralon® of known reflectance R_g using:

$$E_d(\lambda) = \frac{\pi}{R_g(\lambda)} L_d(\lambda) \tag{1}$$

Upwelling radiance L_u was measured using a 3-m long pole which was extended in front of the boat to view undisturbed water ahead of the boat. Sky radiance L_{sky} was measured pointing towards the portion of the sky that would be specularly reflected by a level sea surface in the viewing direction. For each parameter (downwelling irradiance, upwelling radiance and sky radiance), at least 10 measurements were averaged to derive the remote-sensing reflectance R_{rs} [5; 8]:

$$R_{rs}(\lambda) = \frac{L_w(\lambda)}{E_d(\lambda)} = \frac{L_u(\lambda) - \rho L_{sky}(\lambda)}{E_d(\lambda)} \tag{2}$$

where L_w is the water-leaving radiance and ρ is the proportionality factor relating the radiance, measured when the sensor views the sky, to the reflected sky radiance, measured when the radiometer views the sea surface. ρ is hereafter called “reflectance factor”; its value depends on solar zenith angle, on wind speed and on cloud cover [5; 39]. Under clear-sky conditions and wind speeds of less than 10 m/s, ρ is independent of wavelength. At a wind speed of 5 m/s, ρ=0.028. Clouds affect the extent to which ρ depends on wavelength.

SIMBAD is a radiance sensor (field of view = 3°), fitted with a polarizing filter which lets through only the parallel polarized component of observed radiance. At a viewing angle near the Brewster angle, the skylight reflectance at the sea surface is at its minimum. SIMBAD was developed by the Laboratoire d’Optique Atmosphérique de Lille in connection with the Scripps Institute of Oceanography [40]. SIMBAD has 5 channels at wavelengths 443, 490, 560, 670 and 870 nm. For the recommended viewing geometry, i.e. 40° nadir angle (θ_v) and 135° azimuth angle (φ_v) with respect to the sun, the effect of polarization by the sea can be corrected to a few percent despite uncertainties in the optical properties of hydrosols. The protocol recommended for use with the SIMBAD radiometer is described in Fougnie et al. [40].

Fougnie et al. [40], studying the use of polarizers to reduce surface-reflected sky-light, and Mobley [5], using Hydrolight, independently reached the same conclusion: namely, that (θ_v,

#6654 - $15.00 US Received 23 February 2005; revised 13 March 2005; accepted 21 March 2005

φ_v) near (40°, 135°) is optimum. Both protocols were applied with the SIMBAD radiometer and the SD1000 Ocean Optics radiometer during the SARHYGOL cruises across the Gulf of Lions (Table 1). During one of the SARHYGOL campaigns, we used a SIMBADA radiometer, which is identical to the SIMBAD instrument, but with a greater number of channels (11 channels from 350 to 870 nm instead of 5).

Table 1. Characteristics of the reflectance measurements performed during SARHYGOL cruises

Cruise	Dates	SZ [a] Min (deg.)	Nb of SIMBAD scans	Nb of O. Optics scans	Nb of concurrent scans by Simbad and by O. Optics
SARHYGOL 2	25-26 apr 2000	30.1	0	3	0
SARHYGOL 3	14-15 jun 2000	19.7	4 [b]	8	0
SARHYGOL 4	11-12 sep 2000	38.3	9	3	3
SARHYGOL 5	10-11 nov 2000	60.4	5	8	5
SARHYGOL 6	16 feb 2001	55.1	5	7	5
SARHYGOL 8	14-15 jun 2001	19.4	10 [c]	3	0

[a] : Solar Zenith angle - [b] : only L_u - [c] : SIMBADA (11 bands)

3. Separation of Case 1 and Case 2 waters

Surface waters were of two types: Case 2 waters in the Rhône River plume and proximal Region of Freshwater Influence (ROFI) stations, and Case 1 waters at all the other stations (Fig. 1). The reflectance spectra are strikingly different in the Case 1 and Case 2 waters (Fig. 2). Indeed all Case 2 spectra have higher reflectance values in the green than in the blue, which is characteristic of waters rich in phytoplankton, colored dissolved organic matter (CDOM), and detritus. Moreover 7 of the 8 spectra measured in these Case 2 waters exhibit reflectance higher than Case 1 waters reflectance at all wavelengths. The Case 1 waters have their R_{rs} maxima at wavelengths inferior to 500 nm, generally at 443 or 490 nm. These R_{rs} maxima do not exceed 0.007 sr^{-1}. Case 2 waters have their R_{rs} maxima above 500 nm (around 560 nm in our data set). These maxima are as high as 0.025 sr^{-1}, nearly four times higher than the Case 1 waters maxima. In our area, the two waters can quickly be distinguished; for example, $R_{rs}(550) > 0.004$ sr^{-1} for Case 2 waters. Apart from these reflectance differences, Case 2 waters are also characterized by R443/R555 < R443/R510 < R490/R555 < R490/R510 < 1. So both Max (R490/R510, R443/R510) < 1 and Max (R490/R555, R443/R555) < 1 criteria work well to separate the Case 2 waters from the Case 1 waters.

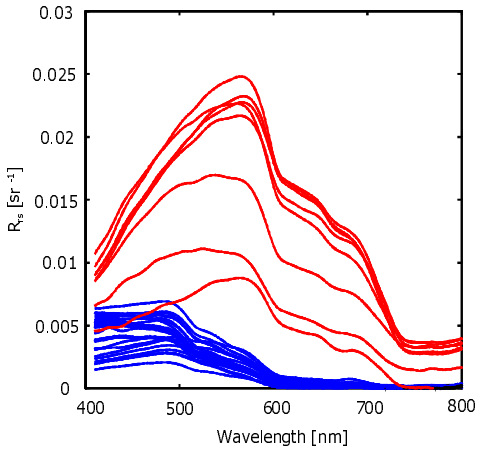

Fig. 2. Remote sensing reflectance spectra collected in the Gulf of Lions with the 8 Case 2 stations in red.

#6654 - $15.00 US
Received 23 February 2005; revised 13 March 2005; accepted 21 March 2005

The Case 2 waters are encountered in the Rhône River plume and in the proximal zone of the ROFI. Waters in the distal zone of the ROFI and outside of the ROFI are Case 1 waters (Table 2). Case 2 waters are strongly influenced by seston and CDOM (not measured in this study). Seston values were higher than 5 $mg.l^{-1}$ in Case 2 waters. The maximum value of total seston was 38.6 $mg.l^{-1}$ and was measured just south of the Rhône mouth. Not surprisingly, these waters could not be separated by their Chl a since those overlapped over the 0.4–1.6 $mg.m^{-3}$ range (for Case 1 waters, Chl a<1.6 $mg.m^{-3}$; and for Case 2 waters, Chl a>0.4 $mg.m^{-3}$). Hereafter, to simplify the sentences, “proximal” will refer to the Case 2 waters and “distal” to the Case 1 waters.

Table 2. Characteristics of the two types of waters considered in this study (24 "distal ROFI" or Case 1 waters, and 8 "proximal ROFI" or Case 2 waters).

Type		Salinity	Chl a (mg/m^3)	Seston [a] (mg/l)	NO_2 (µM)	NO_3 (µM)	PO_4 (µM)
Case 1 waters	Min	37.4	0.06	1.56	0.00	0.02	0.01
	Max	38.2	1.6	3.60	0.25	1.13	0.29
Case 2 waters	Min	8.7	0.4	5.34	0.44	14.74	0.36
	Max	29.6	3.8	38.60	1.41	43.97	0.76

[a] : only 10 measurements

4. Comparison of Ocean Optics and SIMBAD measurements

4.1. Comparison of reflectance values

Concurrent measurements of reflectance were considered of good quality if they were performed within a 5 minutes period, with cloud cover lower than or equal to 2/8 and with wind speed less than 10 m/s, thus enabling a comparison between both measurements. Figure 3 shows one typical example of concurrent reflectance measurements taken from the SARHYGOL 6 experiment. Thirteen cases of these reflectance values were obtained (see Table 1) and will thereafter be referred to as "concurrent reflectance values", without restating the above quality criteria.

These 13 concurrent reflectance values were compared at the three SIMBAD wavelengths below 600 nm (443, 490, 560 nm), as recommended by Mueller et al. [8] (Fig. 4). As both SIMBAD and Ocean Optics R_{rs} measurements were performed concurrently, above-water, and with the same viewing and solar geometry, there is no need to normalize R_{rs} values before comparing them.

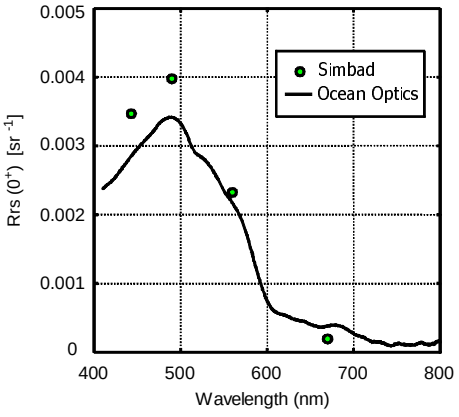

Fig. 3. Example of concurrent reflectance measurements using SIMBAD and Ocean Optics SD1000 radiometers (Gulf of Lions, 16th February 2001).

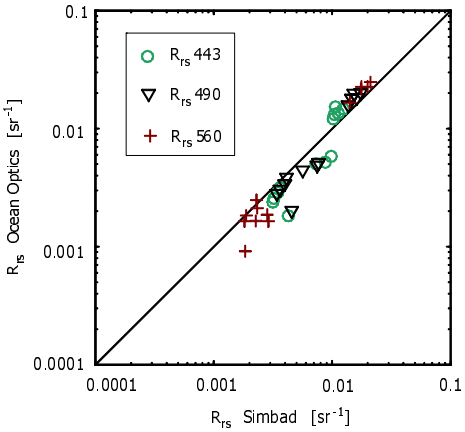

Fig. 4. SIMBAD and Ocean Optics concurrent remote sensing reflectance values at 3 visible wavelengths.

#6654 - $15.00 US Received 23 February 2005; revised 13 March 2005; accepted 21 March 2005

The comparison of the R_{rs} values at SIMBAD wavelengths shows excellent agreement for R_{rs} values higher than 0.01 sr^{-1} at 443, 490 and 560 nm, corresponding to Case 2 waters (Fig. 4). For R_{rs} smaller than 0.01 sr^{-1} (Case 1 waters), the correlation is not as good. The correlation between the two radiometers decreases with reflectance due to the uncertainty on ρL_{sky}. Indeed, this term has more influence on R_{rs} the smaller L_u and R_{rs} are (see eq. 2).

The Ocean Optics measurements were systematically higher than the SIMBAD ones in the Case 2 waters with an averaged difference of 19.4 % (22.2 % at 443 nm, 17.8 % at 490 nm and 18.2 % at 560 nm). This discrepancy between the two R_{rs} estimates is likely explained by the fact that, in the standard SIMBAD treatment, the reflectance at 870 nm is substracted from the reflectance at the other wavelengths to correct for the foam generated by the wind. If this assumption is relevant to Case 1 waters, it is not appropriate in turbid waters [8; 41-42]. Conversely, Ocean Optics reflectance values were weaker than SIMBAD ones in the distal zone or Case 1 waters (away from the plume influence). The average difference between the two reflectance values is 31.9 % (37.6 % at 443 nm, 30.0 % at 490 nm and 28.0 % at 560 nm). This is likely to be explained by our Ocean Optics data treatment because the surface effect correction from a measurement of sky radiance L_{sky} may be very sensitive when applied to clear waters such as those found in distal zones, even at 1/8 or 2/8 cloud coverage. Two main sources of error can affect the surface effect correction: (1) the sky radiance L_{sky} is measured as if it was reflected by a plane air-sea interface, while the latter is not plane; (2) the reflectance factor ρ is considered wavelength independent, while it is not in reality unless the sky is completely cloud-free.

Reflectance ratios exhibit smaller differences, between the two instruments, than the reflectance values (Fig. 5). Since the reflectance factor introduces a bias in the same way (positive or negative) at all wavelengths, this bias is less sensitive in the reflectance ratios than in the reflectance values themselves. The stronger the reflectance values (e.g. in plumes), the less visible the bias. Hence, $R_{rs}(490)/R_{rs}(560)$ ratios (hereafter denoted R490/R560) measured with the two radiometers are very close in the Rhône plume and proximal ROFI (Case 2 waters). Their values are between 0.80 and 0.96 (Fig. 5), their average difference is 1 % and the maximum difference is 1.5 %, while the relative difference between the R490/R560 ratios from both radiometers averages 9.9 % in the distal ROFI. Since the relative difference between the 13 concurrent stations (8 in the distal ROFI, 5 in the proximal ROFI) averages 6.5 %, we consider that the two instruments and their respective protocols are equally good to provide the reflectance band ratios generally used for Chl a derivation.

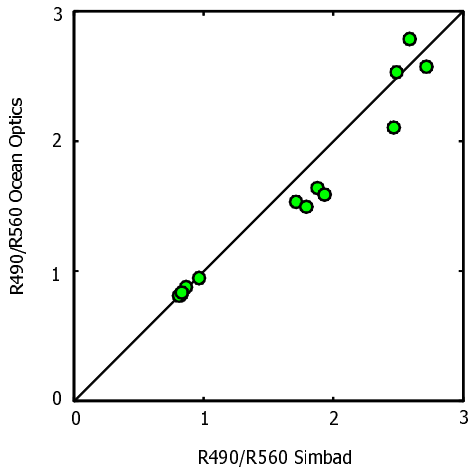

Fig. 5. Comparison of SIMBAD and Ocean Optics concurrent reflectance ratios.

#6654 - $15.00 US Received 23 February 2005; revised 13 March 2005; accepted 21 March 2005

4.2. Comparison of derived Chl a

The ocean chlorophyll 2 algorithm (OC2) and the ocean chlorophyll 4 algorithm (OC4) are, respectively, the two-band and the four-band SeaWiFS operational Chl a algorithms [10]. OC2 and OC4 versions 4 (OC2v4 and OC4v4) were calculated in the third reprocessing of SeaWiFS data from a data set of 2804 stations from oligotrophic up to eutrophic waters [11]. These two algorithms are presented in Table 3.

Table 3. Global and regional Chl a algorithms used in this study. Chl a is expressed in $mg.m^{-3}$.

Name	Ref.	Equation	Chl a range ($mg.m^{-3}$)	R^2	N
OC2v4	[11]	$Chl\,a = 10.0^{(0.319 - 2.336R_{2S} + 0.879R_{2S}^2 - 0.135R_{2S}^3)} - 0.071$ where $R_{2S} = \log_{10}(R490/R555)$	0.008-64	0.883[a]	2,804
OC4v4	[11]	$Chl\,a = 10.0^{(0.366 - 3.067R_{4S} + 1.930R_{4S}^2 + 0.649R_{4S}^3 - 1.532R_{4S}^4)}$ where R_{4S} = max [$\log_{10}$ (R443/R555), $\log_{10}$ (R490/R555), $\log_{10}$ (R510/R555)]	0.008-64	0.892[a]	2,804
GIT96	[14]	$Chl\,a = 0.914 \left[\frac{R440}{R550}\right]^{-1.86}$	0.028-0.36	0.83[b]	21
L-Dorma	[15]	$Chl\,a = 1.49 \left[\frac{R490}{R555}\right]^{-2.51}$	0.07-2	0.948[a]	45
NL-Dorma	[15]	$Chl\,a = 10.0^{(0.217 - 2.728R_{2S} + 0.704R_{2S}^2 + 0.297R_{2S}^3)} - 0.035$ where $R_{2S} = \log_{10}(R490/R555)$	0.07-2	0.941[a]	45
BRI02	[3]	$Chl\,a = 2.094 \left[\frac{R443}{R555}\right]^{-2.357}$	0.034-1	0.952[b]	157
TAS94a	[19]	$\log C = 0.0664 + 0.0462\log(X_{ca}) - 4.144[\log(X_{ca})]^2$ [d] where $X_{ca} = [R443/R555] \,.\, [R412/R490]^{-1.2}$	0.025-1		91[c]
TAS94b	[19]	$\log C = 0.36 - 4.38 \log X_{cb}$ [d] where $X_{cb} = [R443/R555] \,.\, [R412/R490]^{-0.5}$	1-40		-[c]

[a] : calculated from modeled Chl a vs. meas. Chl a - [b] : calculated from log Chl a vs. log R1/R2 - [c] : SeaWiFS reflectance values generated by an optical three-component model adjusted for the summer situation of the Gulf of Naples - [d] : C = Chl a + phaeophytin a concentration

To test OC2v4 with our data, $R_{rs}(555)$ was obtained from SIMBAD $R_{rs}(560)$ or SIMBADA $R_{rs}(565)$ using one of the following empirical relationships derived from the Ocean Optics reflectance spectra (both with R^2=0.9999, N=32):

$$R_{rs}(555) = 0.9898\, R_{rs}(560) + 0.1322 \quad (3.a)$$

$$R_{rs}(555) = 0.9845\, R_{rs}(565) + 0.2660 \quad (3.b)$$

OC4v4 was applied to the Ocean Optics measurements only, as no SIMBAD measurement of $R_{rs}(510)$ was available.

The estimates of Chl a obtained with the OC2v4 algorithm applied to the 13 concurrent Ocean Optics and SIMBAD data are shown in Fig. 6. The derived Chl a smaller than 1 $mg.m^{-3}$ correspond to the stations in the distal ROFI, with the highest R490/R560 ratios (Fig. 5), and show some variability between the two instruments. The derived Chl a is greater than 1$mg.m^{-3}$ at the stations in the proximal ROFI, with a relative difference between the two instruments of less than 3 %. However these results could be misleading: the differences between the derived and measured Chl a for the 13 concurrent R_{rs} measurements are very large (Fig. 7). They show

#6654 - $15.00 US Received 23 February 2005; revised 13 March 2005; accepted 21 March 2005

greater averaged differences in the proximal ROFI (213 % for O. Optics OC2v4, 223 % for O. Optics OC4v4, 214 % for SIMBAD OC2v4) than in the distal ROFI (54 % for O. Optics OC2v4, 53 % for O. Optics OC4v4, 69 % for SIMBAD OC2v4). The difference reaches a factor of 5.7 at one station in the proximal ROFI. When that station is not considered, the averaged differences over the remaining 4 stations in the proximal ROFI are 129 % for O. Optics OC2v4, 137 % for O. Optics OC4v4 and 124 % for SIMBAD OC2v4. The Chl a values derived from the two instruments and using the same algorithm show similar errors compared to the measured values. Other comparisons of global algorithms applied to both Ocean Optics and SIMBAD data would lead to the same conclusion: the algorithms provide similar Chl a estimates using either SIMBAD or Ocean Optics band ratios from the concurrent data set. Thus, one or the other data series can be used for further development; however the algorithms themselves need reworking to be better adapted to the waters of the Gulf of Lions.

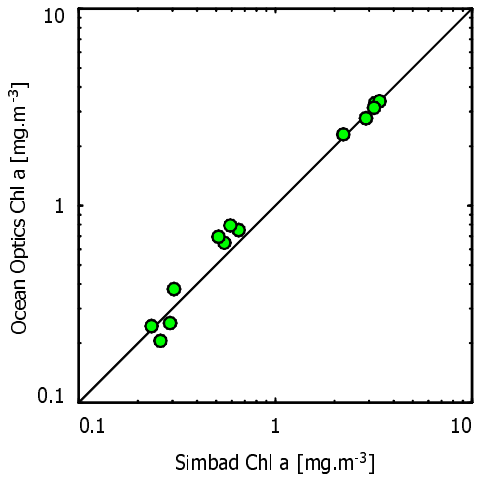

Fig. 6. Comparison of Chl a estimates by SIMBAD and by Ocean Optics using the OC2v4 algorithm [11].

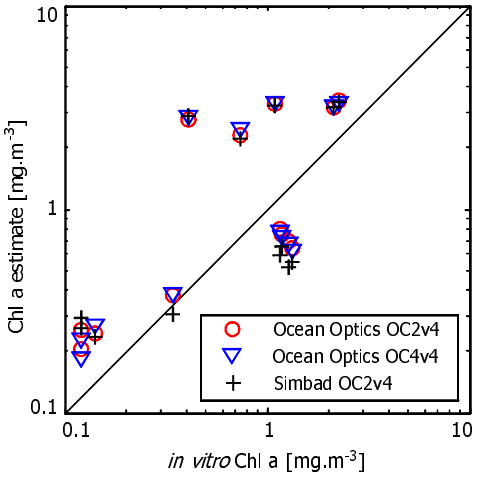

Fig. 7. Chl a estimates using the OC2v4 and OC4v4 algorithms vs. measured Chl a.

5. Chlorophyll *a* algorithms in the Gulf of Lions

We tested Chl a algorithms on the entire set of reflectance spectra collected using the Ocean Optics SD1000 radiometer (32 marine stations, dates in Table 1, locations in Fig. 1, spectra in Fig. 2), as it gave access to more spectral reflectance channels and more band ratios than the SIMBAD radiometer.

5.1. Evaluation criteria

The evaluation of the algorithms is based on criteria used among others by Toole et al. [43] and Darecki and Stramski [44]. Mean and stdev are defined by:

$$\text{mean}(x) = \bar{x} = \frac{1}{n}\sum_{i=1}^{n} x_i \tag{4.a}$$

$$\text{stdev}(x) = \left[\frac{1}{n-1}\sum_{i=1}^{n}(x_i - \bar{x})^2\right]^{1/2} \tag{4.b}$$

From these equations, the mean normalized bias (MNB) and the normalized root mean square (rms) error, in percent, are calculated following:

$$\text{MNB} = \text{mean}\left(\frac{y_{alg} - y_{obs}}{y_{obs}}\right).100 \tag{5.a}$$

#6654 - $15.00 US Received 23 February 2005; revised 13 March 2005; accepted 21 March 2005

$$\text{rms} = \text{stdev}\left(\frac{y_{alg} - y_{obs}}{y_{obs}}\right).100 \quad (5.b)$$

where y_{alg} is a variable obtained from an algorithm and y_{obs} is its value measured *in situ*. MNB is an indicator of systematic error and rms an indicator of random error. Moreover, we calculated mean and stdev values of $\log(y_{alg}/y_{obs})$ data defined by:

$$\text{log\_bias} = \text{mean}\left(\log(y_{alg} / y_{obs})\right) \quad (6.a)$$

$$\text{log\_rms} = \text{stdev}\left(\log(y_{alg} / y_{obs})\right) \quad (6.b)$$

which provide estimates of data scatter for Chl a commonly considered as a lognormally distributed variable [10; 44]. Slope, intercept and the squared correlation coefficient were also calculated for the linear regression of Chl a estimations from various algorithms versus Chl a measurements.

5.2. Global algorithms and two-band algorithms

The algorithms most commonly used to derive Chl a are based on band ratios, for instance R490/R555 (SeaWiFS channels 3 and 5) in the OC2 and OC4 algorithms, R443/R555 (SeaWiFS channels 2 and 5) and R510/R555 (SeaWiFS channels 4 and 5) in the OC4 algorithm. Figure 8 shows measured Chl a versus 2 reflectance ratios. As expected, reflectance ratios decreased when Chl a increased. The dispersion of the reflectance ratios was stronger than the one observed in the datasets used to establish the classic global algorithms (e.g. Ref. [11]). Most of this dispersion is linked to the presence of both Case 1 waters (with R1/R2 > 1 and varying Chl a, see Fig. 8) and Case 2 waters (with R1/R2 ≤ 1). The Chl a algorithms were tested first over the whole of the data, then separately over the distal and the proximal zones (as defined in Section 3).

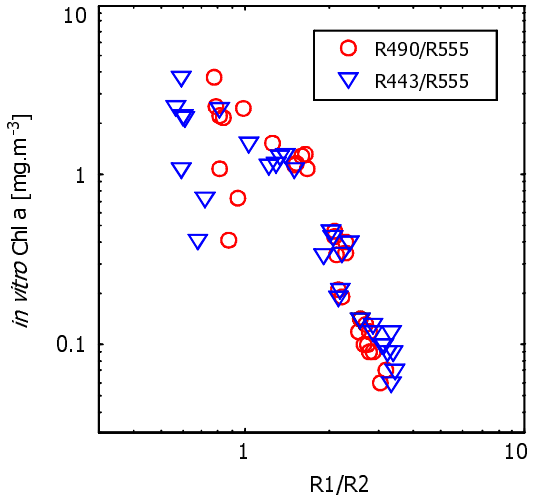

Fig. 8. Measured Chl a vs. reflectance ratios in the Gulf of Lions (N=32).

Global Chl a algorithms OC2 and OC4 were tested on the 32 stations (Table 4). There is little difference in the way they perform. These algorithms do not perform well over the whole data set, compared to results obtained on the complete SeaWiFS calibration data [11]. They yield better results in the distal zone than in the proximal, with a much smaller mean normalized bias, smaller rms and greater R^2. Generally, OC2 and OC4 overestimate Chl a by about 70% for the whole data set, by about 45% in the distal zone, and by a factor of 1.4 in the

#6654 - $15.00 US Received 23 February 2005; revised 13 March 2005; accepted 21 March 2005

proximal zone. As OC2 and OC4 yield similar results, we only presented Chl a values calculated using OC4 versus *in situ* Chl a values for all stations (Fig. 9).

Table 4. Statistical performance of chlorophyll-a algorithms applied to the SARHYGOL dataset (N=32). The parameters are obtained between modeled and measured Chl a.

Zone		OC2v4	OC4v4	GIT96	L-Dorma	NL-Dorma	BRI02	TAS
Global (N=32)	MNB (%)	68.91	72.05	16.73	7.82	13.23	114.37	51.17
	rms (%)	120.76	126.47	83.30	88.06	100.27	238.41	95.51
	log_bias	0.146	0.150	-0.005	-0.053	-0.042	0.206	0.066
	log_rms	0.265	0.271	0.242	0.261	0.273	0.288	0.359
	slope	0.612	0.597	0.840	0.804	0.686	0.277	2.014
	intercept	0.180	0.184	0.180	0.222	0.254	0.305	-0.376
	R^2	0.642	0.639	0.628	0.637	0.632	0.604	0.718
Distal (N=24)	MNB (%)	44.86	46.36	-2.41	-16.02	-16.88	26.79	24.43
	rms (%)	71.75	75.21	42.16	36.89	36.21	38.47	76.13
	log_bias	0.101	0.103	-0.052	-0.121	-0.125	0.083	-0.019
	log_rms	0.242	0.247	0.200	0.210	0.208	0.137	0.360
	slope	0.498	0.491	0.441	0.366	0.372	0.926	0.256
	intercept	0.165	0.168	0.093	0.081	0.078	0.049	0.176
	R^2	0.904	0.884	0.925	0.897	0.887	0.899	0.356
Proximal (N=8)	MNB (%)	141.05	149.13	74.15	79.35	103.58	377.12	131.43
	rms (%)	199.33	207.84	140.93	148.56	166.67	376.38	107.45
	log_bias	0.280	0.293	0.136	0.151	0.208	0.577	0.322
	log_rms	0.303	0.304	0.312	0.304	0.302	0.312	0.212
	slope	0.270	0.263	0.135	0.199	0.262	0.504	2.083
	intercept	2.527	2.619	1.931	1.883	2.092	5.146	0.276
	R^2	0.242	0.269	0.114	0.236	0.247	0.131	0.669

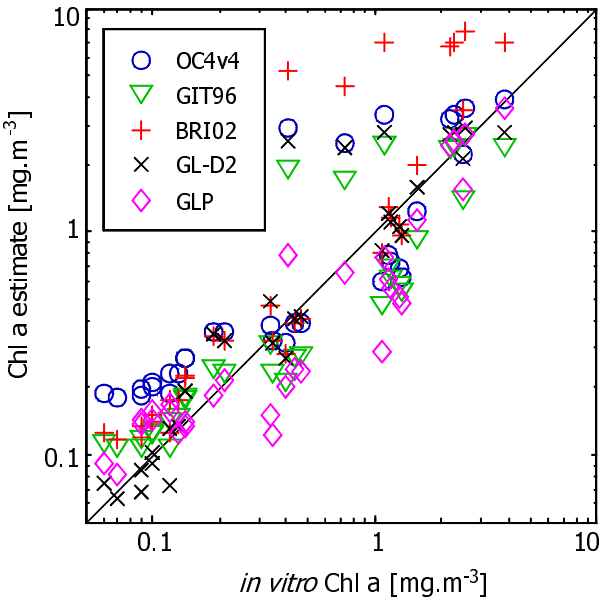

Fig. 9. Estimates vs. *in situ* Chl a by several algorithms on the complete Sarhygol dataset (distal + proximal ROFI).

#6654 - $15.00 US
Received 23 February 2005; revised 13 March 2005; accepted 21 March 2005

5.3. Test of regional Chl a algorithms

The present section tests the Mediterranean regional algorithms used by other authors. Their complete equations are given in Table 3. The GIT96 algorithm [14] was established for the CZCS bands from 21 coastal stations near Gaza, in the southeastern Mediterranean Sea. The L- and NL-Dorma algorithms [15], which concern the SeaWiFS bands, were derived from 45 stations in Case 1 waters of the western Mediterranean Basin. Bricaud et al. [5] suggested another algorithm (BRI02; SeaWiFS bands) using 157 stations in various locations through the Mediterranean Sea. The only regional algorithm, specifically applicable to coastal areas, was derived by Tassan in 1994 [19] (TAS94) from SeaWiFS reflectance values and adjusted to the summer situation of the Gulf of Naples, Italy. TAS94 is a 4-band algorithm, the others are based on a single band ratio.

The GIT96, L- and NL-Dorma algorithms perform very similarly, whether over the entire Gulf of Lions, or over each zone separately (Table 4). They generate a mean normalized bias of less than 17% over the whole data set. This conceals a large disparity between the two water masses in the Gulf of Lions. Whereas OC2 and OC4 tend to overestimate Chl a in both zones, GIT96, L- and NL-Dorma underestimate Chl a by up to 17 % in the distal zone, and overestimate it by 74 to 103 % in the proximal zone. In the distal zone, GIT96 reduces significantly the MNB (-2.4 %) but the slope of the linear regression between modeled and measured Chl a is inappropriate (0.44).

By comparison, BRI02 performs better than the above algorithms in the distal zone, and worse in the proximal zone. In the distal zone, BRI02 has similar values of rms and R^2 as the others, a mean bias of 27% and a far better slope of 0.926 (instead of less than 0.5). However, in the proximal zone, it performs less well than the other algorithms (average error of a factor of 3.8). Figure 9 shows the Chl a values calculated using OC4, GIT96 and BRI02 over the whole study area. As clearly seen, there is a strong dispersion in the results and no model seems to be perfect for the data.

Nonetheless, TAS94 behaves differently than the other algorithms discussed here. It generates relatively small average errors, but rms higher than most of the other algorithms. It shows a very large dispersion of Chl a estimates over each zone and overestimates Chl a in both water types. In fact, the usefulness of this algorithm does not lie in the quality of its performance but in its high R^2 value. Indeed, the R^2 value which it generates, for the proximal zone, is much higher than the other algorithms. This suggests the relevance, for this proximal zone, of the intermediate parameter X_c, defined as:

$$X_c = \frac{R443}{R555} \cdot \left[\frac{R412}{R490} \right]^{+n} \tag{7}$$

where n is equal to (-1.2) for Chl a < 1 $mg.m^{-3}$ (giving X_{ca}), and is equal to (-0.5) for 1 < Chl a < 40 $mg.m^{-3}$ (giving X_{cb}). The first term R443/R555 is Chl a sensitive since the numerator wavelength corresponds to the Chl a absorption maximum and the denominator wavelength to the Chl a absorption minimum. The second term R412/R490 is seston and CDOM sensitive. It is not very sensitive to Chl a since it is the reflectance ratio of two wavelengths that are on either side of the Chl a absorption maximum.The adaptation of a Chl a algorithm based on X_c in the proximal zone is further studied in part 5.5.

5.4. Algorithms for the distal ROFI

Among the two-band algorithms we tested on the distal ROFI, BRI02 gave the closest agreement with *in situ* concentrations: the averaged error was 26.8%, R^2 (0.899) was among the highest values, and the slope was, by far, the closest to 1 (0.926, the second higher value being 0.498 for OC2v4 – see Table 4). BRI02 is based on the band ratio R443/R555. Limiting our calculations to the distal zone data, we established the empirical algorithm giving the best-fit between measured R443/R555 and measured Chl a. The resulting algorithm, called hereafter **GL-D1** (Gulf of Lions, Distal area 1), is defined by:

#6654 - $15.00 US Received 23 February 2005; revised 13 March 2005; accepted 21 March 2005

$$\text{Chl}\,a = 2.513\left[\frac{R443}{R555}\right]^{-2.827} \quad (8)$$

Its performance is slightly better than BRI02: R^2 is nearly as good (0.867 instead of 0.899) and the mean normalized bias is 3.3% instead of 26.8%, the slope is also close to 1 (see Table 5 and Fig. 10). Based on the same band ratio R443/R555 but with a power law rather than an exponential one, the alternative algorithm –called **GL-D2** – is:

$$\text{Chl}\,a = 6.258\ .exp\left(-1.344\left[\frac{R443}{R555}\right]\right) \quad (9)$$

Table 5. Statistical performance of optimized Chl a algorithms at SeaWiFS bands for the SARHYGOL dataset (N=32). The parameters are obtained between modeled and measured Chl a.

Zone		GL-D1	GL-D2	GLP
Global	MNB (%)	153.07	31.82	-5.97
(N=32)	rms (%)	368.56	104.25	44.67
	log_bias	0.186	0.056	-0.081
	log_rms	0.374	0.206	0.230
	slope	3.326	0.914	0.899
	intercept	-0.115	0.230	-0.076
	R^2	0.585	0.666	0.869
Distal	MNB (%)	3.33	3.67	
(N=24)	rms (%)	26.62	29.67	
	log_bias	$2.2\ 10^{-6}$	$-2.6\ 10^{-5}$	
	log_rms	0.115	0.117	
	slope	1.072	0.865	
	intercept	-0.028	0.037	
	R^2	0.867	0.946	
Proximal	MNB (%)			5.53
(N=8)	rms (%)			39.80
	log_bias			$-3.45\ 10^{-6}$
	log_rms			0.48
	slope			0.902
	intercept			0.141
	R^2			0.851

GL-D2 is the best algorithm in the distal zone of the Gulf of Lions at the SeaWiFS wavebands (Fig. 10). It has the highest R^2, and a bias and rms similar to the other algorithms (Tables 4 and 5). In fact, it also provided the closest agreement with *in situ* concentrations for the entire data set (distal and proximal) with an averaged error of 31.8%, a similar R^2 and the closest slope to 1 (0.914 – see Table 5). The equivalent algorithms at the MODIS wavebands (443 and 550 nm) and at the MERIS wavebands (443 and 560 nm) are:

$$\text{Chl}\,a = 7.113\ .exp\left(-1.496\left[\frac{R443}{R550}\right]\right) \quad (10.a)$$

$$\text{Chl}\,a = 5.677\ .exp\left(-1.221\left[\frac{R443}{R560}\right]\right) \quad (10.b)$$

#6654 - $15.00 US Received 23 February 2005; revised 13 March 2005; accepted 21 March 2005

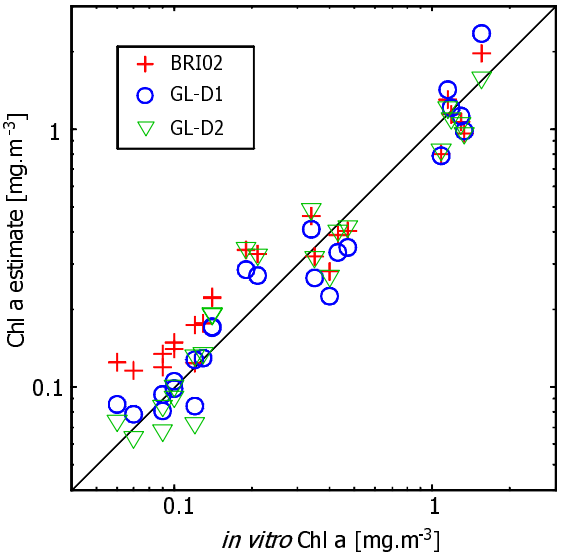

Fig. 10. Estimated vs. *in situ* Chl a in the distal Rhône ROFI using several algorithms.

5.5. Algorithms for the proximal ROFI

Among the published algorithms, TAS94 is the one which gives the best R^2 and thus the most linear relationship between the measured and modeled values for Chl a in the proximal ROFI (Table 4). However, its rms is high compared to the others. This suggests that X_c or a close parameter is useful to estimate Chl a in coastal zones, but that the numerical coefficients (multipliers and indices) used in TAS94 need to be adapted.

Regressions of Chl a against X_c, X_{ca}, X_{cb} for the sub-population of proximal ROFI data (data not shown) indicate that the Chl a limit used in their definition (1 mg.m^{-3}, see Table 3) could be slightly modified in our data. Hence X_{cmod} is introduced as:

$$X_{cmod} = X_{ca} \qquad \text{for } 0.025 < \text{Chl a} < 1.1 \text{ mg.m}^{-3} \tag{11.a}$$

$$X_{cmod} = X_{cb} \qquad \text{for } 1.1 < \text{Chl a} < 40 \text{ mg.m}^{-3} \tag{11.b}$$

The algorithm using X_{cmod} in the proximal waters, called GLP, is defined by:

$$\text{Chl a} = 1.609 \; X_{cmod}^{\;-\,2.457} \tag{12}$$

This relationship is shown on Fig. 11. Figure 12 shows a comparison between *in vitro* Chl a and Chl a estimated by this algorithm and by L-Dorma (see statistical performance in Table 4). GLP statistics are better than those of the others for the proximal ROFI zone, with the lowest MNB, the lowest rms, the highest R^2 and the closest slope to 1.

Taking into account the large dispersion of Chl a for R1/R2 ≈ 1 in the proximal ROFI (Fig. 8), single band ratios are not suitable for deriving Chl a with our data set. Indeed, the best correlation factor R^2 between a reflectance ratio (R510/R550) and Chl a in the proximal ROFI zone was 0.183. It has already been shown that the correlation between the blue/green band ratios and surface chlorophyll concentration held only at stations where yellow substance was not present (e.g. Ref. [45]). Thus X_c or a derived parameter such as X_{cmod} seems to be a more suitable parameter than any single band ratio for deriving Chl a in the proximal ROFI zone.

In fact, GLP is not only good in the proximal ROFI zone but on the entire data set (Table 5). Its performances (MNB = -6%, rms < 45%, slope = 0.899, R^2 = 0.869) are better than those of all the other algorithms (except for the GL-D2 slope). This proves that the

#6654 - $15.00 US Received 23 February 2005; revised 13 March 2005; accepted 21 March 2005

parameter X_{cmod} is extremely useful to derive Chl a, not only in the proximal ROFI but also in both Case 1 and Case 2 waters. However, some caution is needed here, as these results were obtained from a small data set in the Gulf of Lions, and must be considered as preliminary. A major limit of the X_{cmod} parameter is that it requires to know, *a priori* and for each point of measurement, wether Chl a exceeds or not the 1.1 $mg.m^{-3}$ threshold value.

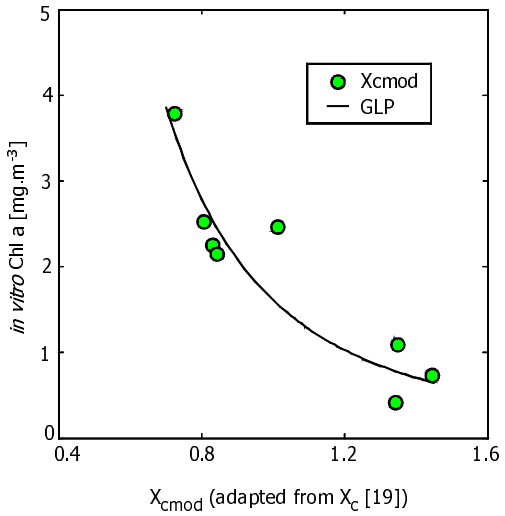

Fig. 11. Chl a vs. X_{cmod} in the proximal Rhône ROFI and regression relationship.

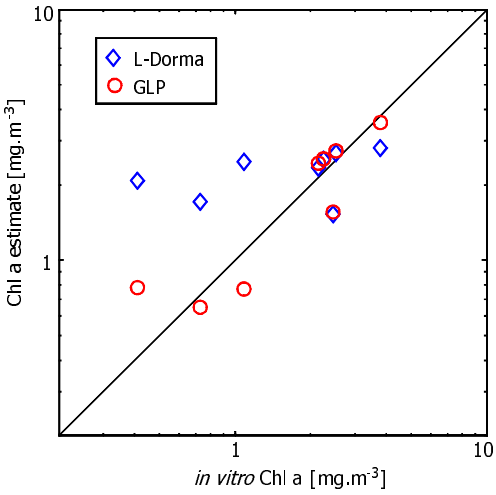

Fig. 12. Modeled Chl a vs. *in situ* Chl a in the proximal Rhône ROFI using two algorithms.

6. Discussion and conclusion

The variability of reflectance ratios in the Gulf of Lions is mostly due to the spatial variability of hydrological features within that area [29; 46]. The dispersion of the commonly used band ratios is stronger than the ones observed in the datasets used to establish the global algorithms, such as the one used by O'Reilly et al. [11]. A large part of the dispersion seems to be linked to the location of the measurements, and the resulting points can easily be separated into two distinct groups: Case 1 waters in the plume and the proximal ROFI and Case 2 waters in the distal ROFI and the rest of the Gulf of Lions.

The reason for the strong difference between the two groups of points is likely twofold: First, plume and proximal ROFI waters carry higher amounts of dissolved substances and suspended particles than offshore waters, making reflectance ratios in these zones strongly influenced by other optically-significant components than chlorophyll [47-49]. For instance, it has been shown that reflectance in the vicinity of 550 nm, used in Chl a algorithms, is best able to quantify suspended particles in moderately turbid coastal waters [50-51]. Second, the dominant kinds of phytoplankton organisms living in the distal zone are different from those in the proximal zone. Plankton is dominated by nanoflagellates in the Rhône River plume, and by diatoms in the dilution zone [29]. Variability of phytoplankton populations, with different optical signatures (e.g. Ref. [52-54]), likely introduces dispersion in the reflectance ratios. Moreover, changes in the absorption to scattering ratio, due to changes in phytoplankton growth [55] in a ROFI zone may also disturb reflectance ratios, even at equal chlorophyll concentrations.

Other sources of reflectance variability include temporal variations of the different components present in the water and detailed above, and all the physical processes influencing the Gulf of Lions circulation and vertical structure. For example, Banzon et al. [56] found a remarkable correlation between surface chlorophyll fluctuations and mixed layer depths in the Southern Adriatic, western Mediterranean Sea.

#6654 - $15.00 US Received 23 February 2005; revised 13 March 2005; accepted 21 March 2005

In any case, it was surprising to see that the proximal and distal waters could be distinguished as easily by both the two following criteria : Max (R490/R510, R443/R510) < 1, and Max (R490/R555, R443/R555) < 1. It may be due to the strong reflectance differences between the two groups of points. This should be further investigated both in the Gulf of Lions and in other coastal regions.

We must point out that the algorithms presented in this paper were obtained using a relatively small data set, especially in the proximal ROFI, and should be tested, and eventually refined, on a larger data set. Nonetheless, our results clearly show that, although two-band algorithms are satisfying in the distal zone, more specific algorithms are needed in the proximal ROFI zone in the Gulf of Lions. Indeed, in the distal zone, the algorithm presented by Bricaud et al. [5] gave the best performance among the published algorithms we tested. But in the proximal zone, we suggest not to use algorithms based on a single band ratio and we recommend the use of an intermediate parameter, based on 4 reflectance values, as proposed by Tassan [19]. Other methods could also be considered, such as the simultaneous inversion of several parameters (Chl a, CDOM, seston) based on multi-spectral data, possibly adapted to each type of coastal waters (e.g. Ref. [57]).

Acknowledgments

This study was financed by the French scientific '*Programme National Environnement Côtier*' (PNEC, *Chantier Golfe du Lion*) and '*Programme ATmosphère Ocean à Moyenne échelle*' (PATOM, SARHYM experiment). The authors thank J. Gaggelli from LSEET, Toulon, for his help on reflectance measurements, N. Garcia and P. Rimmelin from LOB, Marseille, who performed the chlorophyll measurements, and P.-Y. Deschamps, F. Thieuleux and G. Becu from LOA, Lille, for the SIMBAD data analysis. The authors are also grateful to the crews of the RV Téthys II.